GEOLOGIC MAPPING AND STUDIES OF DIVERSE DEPOSITS AT NOCTIS LABYRINTHUS, MARS.

Catherine M. Weitz[1], Dan Berman[1], Alexis Rodriguez[1], and Janice L. Bishop[2], [1]Planetary Science Institute, 1700 E Fort Lowell, Suite 106, Tucson, AZ 85719 (weitz@psi.edu); [2]SETI Institute, 189 Bernardo Ave., Mountain View, CA 94043.

Introduction: Noctis Labyrinthus consists of a network of intersecting linear troughs and pits along the eastern Tharsis rise that connect eastward to the continuous chasmata of Valles Marineris. The pits and troughs may have formed due to withdrawal of magmatic reservoirs at depth [1], or by collapse over conduits developed as a consequence of groundwater flow along pre-existing fault systems [2]. The age of the Noctis Labyrinthus depressions is thought to be Late Hesperian to Early Amazonian based upon disruption of the lava plains along the plateaus [3-5]. Consequently, sediments deposited within the depressions represent this age or younger materials.

Mapping Investigation: For this study, we are mapping the western portion of Noctis Labyrinthus (-6 to -14°N, -99.5 to -95.0°W; Fig. 1), which includes some of the most diverse mineralogies identified on Mars using CRISM data [6-9]. We are using THEMIS daytime IR as a basemap, with a 1:500,000 publication scale. Thus far across the Noctis Labyrinthus region, the following minerals have been identified in association with light-toned deposits (LTDs): several kinds of sulfates (monohydrated {kieserite, szomolnokite} and polyhydrated sulfates, jarosite, and Ca-sulfates {gypsum, basanite}, clays {Fe/Mg-phyllosilicates and Al-phyllosilicates}, a doublet absorption between 2.2-2.3 μm, and hydrated silica/opal. The role of water, both in the formation of the Noctis depressions and the hydrated deposits found within them, is a focus of this investigation. The diverse range of sulfates and phyllosilicates identified within the depressions of Noctis Labyrinthus either resulted from localized aqueous activity [8,9] and/or may have been part of a broader synoptically driven period of late activity during the Late Hesperian to Amazonian [e.g., 10-12].

Mapping Progress: We have completed mapping of all geologic units and linear features (Fig. 1). Numerous structural features, including grabens and scarps, are found throughout the mapping region. Mapping of normal faults and grabens indicates multiple episodes of collapse.

Loose eolian debris and dust covers much of the plateau, trough floors, and wallrock, obscuring geologic contacts between different units at these locations. The dust mantle thins to the east and south, where individual lava flows are evident along the plateau. Two volcanic shields have been mapped in the southwestern plateau and both are embayed by younger lava flows. Beneath the plateau plains unit is the gullied and layered wallrock unit, which is similar in morphology to the layered gullied upper wallrock observed throughout Valles Marineris. Light-toned deposits occur in only one location along the plateau and they are only visible as small patches because a dark mantle and eolian ripples cover much of the plateau, including the light-toned deposits, in this region. CRISM spectra show the presence of opal in association with these plateau deposits.

Floor units within the troughs and pits include light-toned deposits, many of which also exhibit spectral hydration features, and mass wasting deposits, including landslides. Lava flows with Amazonian ages [13] have been mapped on two trough floors. Floor morphology can either be smooth or rough, with the smooth morphology typically the result of eolian fill. No fluvial channels have yet been identified either along the plateau or within the depressions, but a possible volcanic channel sourced by a collapsed rounded depression within one of the troughs indicates younger volcanism occurring after formation of the trough. Dark dunes have been mapped in two troughs.

Relative dating of surfaces employed crater statistics and stratigraphic relationships, where crater statistics were compiled in ArcGIS using a subset of CTX images and CraterTools, a plug-in software for ArcGIS [14]. The resolution of CTX images enabled confident definition of craters >20 m in diameter (D) and counts excluded obvious secondary clusters. Interpreted absolute ages for each count were derived from segments of the plots for each unit that best match the expected production population using "root-2" binned differential histograms and Craterstats2 software [15]. Absolute derived ages are based on the production function of [16] and chronology function from [17, 18]. The geologic epoch associated with each count and range of epochs covered by the error bars are based on the chronology function from [18]. Randomness analyses [19] were also included to ensure lack of clustering.

References: [1] Mege D. et al. (2003) *J. Geophys. Res*., 108(E5), doi:10.1029/2002JE001852; [2] Rodriguez, J.A.P. et al. (2016) *Planetary and Space Science*, *124*, 1-14. [3] Tanaka K.L. and P.A. Davis (1988) *J. Geophys. Res. 93*, 14893-14917; [4] Witbeck et al., (1991) USGS Map I-2010, scale 1:2,000,000; [5] Tanaka K.L. et al. (2014) Geologic Map of Mars, *USGS Map* 3292; [6] Weitz C.M. and J.L. Bishop (2014) *Mars 8th Conference*, Abstract 1222; [7] Weitz C.M. and J.L. Bishop (2013) *Planet. Space Sci*., doi:10.1016/j.pss.2013.08.007; [8] Weitz C.M. et al. (2011) *Geology*, 39;899-902, doi: 10.1130/G32045.1; [9] Thollot P.

et al. (2012) *J. Geophys. Res.*, 117, E00J06, doi:10.1029/2011JE004028; [10] Moore J.M. and A.D. Howard (2005) *J. Geophys. Res., 110*, E04005, doi:10.1029/2005JE002352; [11] Fassett C.I. and J.W. Head (2008) *Geophys. Res. Letts.*, *32*, L14201, doi:10.1029/2005GL023456; [12] Grant J.A. and S.A. Wilson, (2011) *Geophys. Res. Letts.*, 38, L08201, doi:10.1029/2011GL046844. [13] Mangold N. et al. (2009) Earth Planet.. Sci. Letts. 294, 440-450. [14] Kneissle, T. et al. (2016) *PSS*, *59*, 1243-1254. [15] Michael, G.G., and G. Neukum, (2010) *EPSL*, doi:10.1016/j.epsl.2009.12.041. [16] Hartmann, W.K. and I.J. Daubar (2017), *Meteor. & Planet. Sci.*, 52(3), 293-510. [17] Hartmann WK (2005) Icarus 174, 294-320. [18] Michael GG (2013) *Icarus* 226, 885-890. [19] Michael GG et al. (2012), *Icarus*, 218(1), 169-177

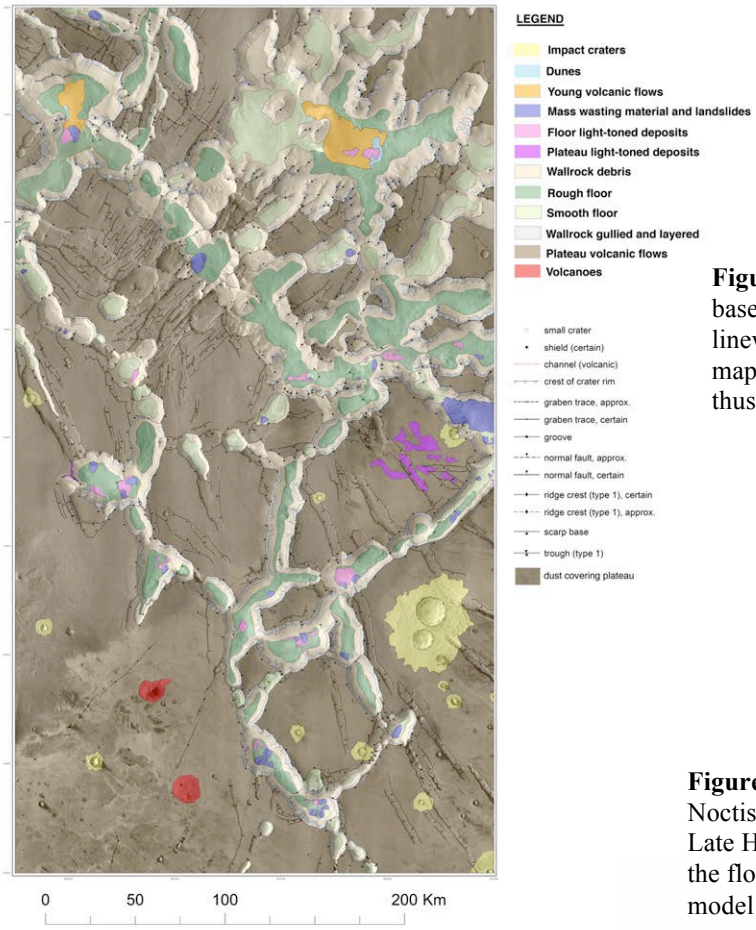

Figure 1. THEMIS daytime IR basemap with geologic units and linework overlain for our geologic mapping region in Noctis Labyrinthus.

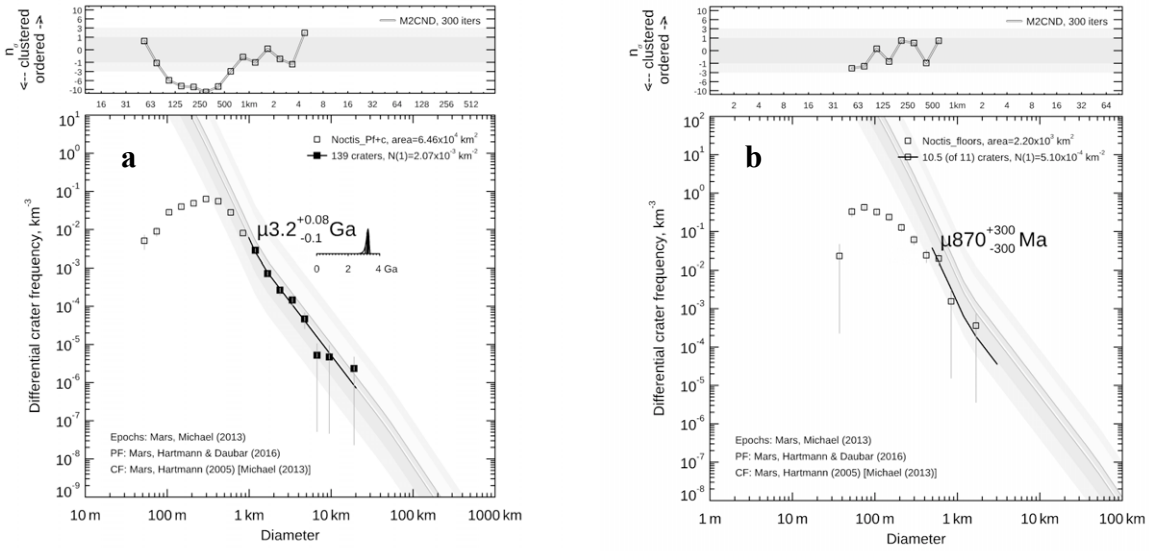

Figure 2. (a) Crater size frequency for the Noctis plateau that shows a model age of Late Hesperian. (b) Crater size frequency for the floors of the pits and troughs that shows a model age of Amazonian.